

Effect of Cathodic Polarization on Corrosion Behavior of X65 Steel in Seawater Containing Iron-oxidizing Bacteria

Meiying Lv, Yongyong Yue, Zhenxin Li, Min Du*

Key Laboratory of Marine Chemistry Theory and Technology, Ministry of Education, College of Chemistry and Chemical Engineering, Ocean University of China, Qingdao 266100, P.R. China

*E-mail: ssdm99@ouc.edu.cn

Received: 8 September 2020 / Accepted: 30 October 2020 / Published: 30 November 2020

Microbiologically influenced corrosion is mainly caused by the biological activity in the biofilm, which clearly illustrates the role of attached bacteria in the form of biofilm in initiating or accelerating corrosion. Although it has been proven that electrochemical methods can prevent the formation of biofilms on metal surfaces, the special effect of cathodic polarization in bacterial attachment and growth is still inconclusive. The purpose of this work was to investigate the effect of cathodic polarization on the attachment of iron-oxidizing bacteria (IOB) in seawater during the initial stage of biofilm formation. Results showed that under the polarization potential of $-1050\text{ mV}_{\text{vs. SCE}}$, IOB attachment and biofilm growth were well controlled. Further, the potential of $-1050\text{ mV}_{\text{vs. SCE}}$ exhibited more effective inhibitory effect on IOB-induced pitting corrosion than that of $-700\text{ mV}_{\text{vs. SCE}}$, which was related to the accumulation of electrons on the metal surface during cathodic polarization. The cathodic potential of $-1050\text{ mV}_{\text{vs. SCE}}$ also altered the electrochemical parameters at the metal-biofilm interface, such as the increase of pH and the formation of protective calcareous deposits, which contributed to protect the metal from IOB-induced corrosion.

Keywords: Microbiologically influenced corrosion; Cathodic polarization; Iron-oxidizing bacteria; Bacterial attachment; Biofilm

1. INTRODUCTION

Iron-oxidizing bacteria (IOB), as the main aerobic bacteria in microbiologically influenced corrosion (MIC) research, are known as metal depositing microorganisms that are able to deposit iron hydroxides extracellularly [1, 2]. IOB can obtain the energy by oxidizing iron to maintain their metabolism [3]. They oxidize ferrous ions (Fe^{2+}) to ferric ions (Fe^{3+}) much faster than conventional chemical oxidation [4]. Our previous studies also indicated that IOB accelerate the dissolution and local corrosion of metals [5].

Effects of cathodic polarization on corrosion inhibition of aerobic bacteria have been paid much attention. For example, Shim et al. [6] studied the inhibitory effect of electric currents on the adhesion of *Pseudomonas aeruginosa* on the surface of transparent indium-tin-oxide (ITO) coated glass. With the negative currents from 0 to 15.0 $\mu\text{A}/\text{cm}^2$, the numbers of adhered cells decreased to 19%, which can be interpreted as an effect of electrostatic repulsion between the negatively charged bacteria and the cathode surface. Hong et al. [7] showed that the detachment ratio of *Pseudomonas aeruginosa* on the ITO-coated glass surface was approximately 80% after applying a cathodic current of 15.0 $\mu\text{A}/\text{cm}^2$. However, due to the uneven distribution of the binding force between the bacteria and the electrode surface, about 20% of the bacteria cells still survived. Upon the application of cathodic polarization, oxygen depolarization on the cathode surface may have two different pathways: 4-electron process and 2-electron process [8]. Thus, it is possible to generate hydroxyl ions (OH^-) or hydrogen peroxide (H_2O_2) by the electro-reduction of oxygen. The generation of H_2O_2 has been investigated for decades to control bacterial growth. DeQueiroz et al. [9] showed that when *Pseudomonas aeruginosa* was treated with H_2O_2 , there were a large number of perforations in the cell walls and cell membranes. This was because H_2O_2 caused the destruction of cell membrane components by destroying the thiol groups in the enzyme. Istanbulu et al. [10] studied the electrochemical biofilm control mechanism of *Pseudomonas aeruginosa* on 316L stainless steel surface. It was pointed out that when the metal sample was polarized to $-600\text{ mV vs. Ag}/\text{AgCl}$, the production of H_2O_2 near the electrode surface was the key to control the growth of biofilm. However, due to the low concentration of H_2O_2 , it was difficult to detect in the solution. In addition, Eashwar et al. [11] claimed that the formation of OH^- at the cathode polarized interface was the main reason for the inhibition of biofilm accumulation and activity.

In fact, 2-electron and 4-electron reactions exist simultaneously in the process of cathodic oxygen reduction, which depend on the type of electrode material and the applied potential. For some materials with low catalytic activity, 2-electron pathway was initially the dominant reaction. At more negative potentials, as it reaches the overpotential for complete reduction to OH^- , 4-electron pathway has a great contribution to the total cathode current. To clarify the antibacterial mechanism of cathodic polarization, it is important to understand the dominant reaction on the cathode surface. In this work, the corrosion behavior of X65 steel under the polarization potential of -700 mV vs. SCE and -1050 mV vs. SCE in seawater containing IOB was investigated. The benefit of this work is to reveal the electrochemical control mechanism of the IOB induced MIC, which provides a valuable reference for the future work of cathodic polarization in marine environment.

2. EXPERIMENTAL

2.1 Coupon preparation

Corrosion coupon used for this work was X65 pipeline steel, with a composition (wt.%): C (0.03), Si (0.17), Mn (1.51), P (0.02), Ni (0.17), Cu (0.04), Mo (0.16), Nb (0.06), Al (0.02), Ti (0.01)

and Fe (balance). The $10 \times 10 \times 3$ mm coupons were embedded in epoxy resin with the exposed area of 1 cm^2 , and a copper wire was connected to each coupon for electrochemical measurements. The coupons with $50 \times 10 \times 3$ mm were used for weight loss test and morphology characterization. All the steel coupons were successively sanded with different types of SiC metallurgical papers (400, 600, 800, 1000 and 2000-grit). Subsequently, the coupons were washed with absolute ethanol, dried in high-purity N_2 (99.999%) and sterilized with an ultraviolet lamp for 30 min before using.

2.2 Bacteria cultivation

IOB (*Pseudomonas sp.*) were isolated from the carbon steel rust layer immersed in seawater near the Qingdao (China) and identified by polymerase chain reaction (PCR) amplification of 16S rDNA. The IOB cultures were inoculated in culture medium containing the following components: 0.5g K_2HPO_4 , 0.5g NaNO_3 , 0.2g CaCl_2 , 0.5g $\text{MgSO}_4 \cdot 7\text{H}_2\text{O}$, 0.5g $(\text{NH}_4)_2\text{SO}_4$ and 10g ammonium iron citrate and 1L natural seawater (pH 7.2 ± 0.1). The culture medium was autoclaved at 121°C for 20 min before using. IOB strains cultured for 5d were inoculated into 500 mL test solution (1% v/v). The test solution was sterile seawater containing total nutrient medium.

2.3 Weight loss tests

After 21d, the coupons were taken out from the test solution and immersed in the pickling solution containing corrosion inhibitor (hexamethylenetetramine) for 5 min to remove the corrosion products and biofilms. After that, the coupons were washed with distilled water, dehydrated with absolute ethanol, and dried using N_2 stream. The corrosion rate (V_{corr}) of X65 steel was calculated by the following formula:

$$V_{\text{corr}} = \frac{(m_1 - m_2) \times 10^6}{st} \quad (1)$$

where V_{corr} , s and t are corrosion rate ($\text{g} \cdot \text{m}^{-2} \cdot \text{h}^{-1}$), exposed area (mm^2) and corrosion time (h), respectively. m_1 is the weight of iron coupon before immersion in the test solution, and m_2 is the weight of iron coupon after 21d of immersion.

2.4 Surface analysis

Prior to scanning electron microscopy (SEM, JSM-6700F, Japan) and energy dispersive X-ray spectrum (EDS) testing, the coupons were pretreated with phosphate buffer solution (PBS) containing 5% glutaraldehyde (v/v) for 2h to immobilize cells and then dehydrated with different concentrations of ethanol (30%, 50%, 70%, 90% and 100% in v/v). Finally, the coupons were dried using N_2 stream and coated with a thin gold film to provide electrical conductivity. The fluorescence images were taken using an Olympus microscope (Olympus, U-RFL-T, Japan). Prior to observation, the coupons were also pretreated with PBS solution containing glutaraldehyde, and then stained with a fluorescent dye (4', 6-diamidino-2-phenylindole, DAPI) for 30 min in the darkness. The elemental composition of the corrosion products was examined by X-ray photoelectron spectroscopy (XPS, ESCALAB 250Xi, Thermo Fisher, USA). The confocal laser scanning microscope (Keyence, VK-X200, Japan) was used

to characterize the surface morphology of X65 steel after removing the corrosion products and biofilms.

2.5 Electrochemical measurements

In this work, electrochemical measurements were performed using a Gamry electrochemical workstation (Reference 600, USA) in a conventional three-electrode system, with iron coupon as the working electrode, platinum plate as the counter electrode, and saturated calomel electrode (SCE) as the reference electrode. A potentiostat (HWL-1) was used to perform cathodic polarization of X65 steel for 21d at the potentials of -700 and -1050 mV vs. SCE. Electrochemical impedance spectroscopy (EIS) was measured at a steady-state open circuit potential (OCP) after cathodic polarization using sinusoidal voltage signal of 10 mV in the frequency range of 10^5 to 10^{-2} Hz. First, the applied polarization potential was turned off for about 40 min to return the OCP to a steady state, and then EIS measurement was performed. After the EIS test was completed, the polarization potential was immediately reapplied to the metal electrode. The Zview2 software (Scribner Inc.) was employed to fit the EIS data using the equivalent circuit model. Potentiodynamic polarization curves were determined ranging from -200 mV to $+300$ mV (vs. OCP) at a sweep rate of 0.5 mV/s. The experimental data were analyzed using Cview2 software (Scribner Inc.). The local pH around the iron coupon was detected by Ir/IrO₂ electrode. All measurements were conducted at 25 °C and repeated at least 3 times.

3. RESULTS AND DISCUSSION

3.1 Selection of cathodic polarization potential

Fig. 1 showed the cathodic potentiodynamic polarization curve of X65 steel in seawater containing IOB. It can be seen that the corrosion potential was -462.6 mV vs. SCE. Moreover, the hydrogen evolution potential was observed to be about -952.8 mV vs. SCE. Therefore, we chose the potential of -700 mV vs. SCE in the process of cathode oxygen diffusion between -462.6 mV vs. SCE and -952.8 mV vs. SCE. Generally, the cathodic protection criteria in the marine environment was not negative than -1050 mV vs. SCE to prevent hydrogen embrittlement. Herein, the potential of -1050 mV vs. SCE was selected as another applied potential. And our previous studies showed that the growth cycle of IOB was about 14d, so we chose 21d of testing to evaluate the longer-term effect of cathodic polarization [5].

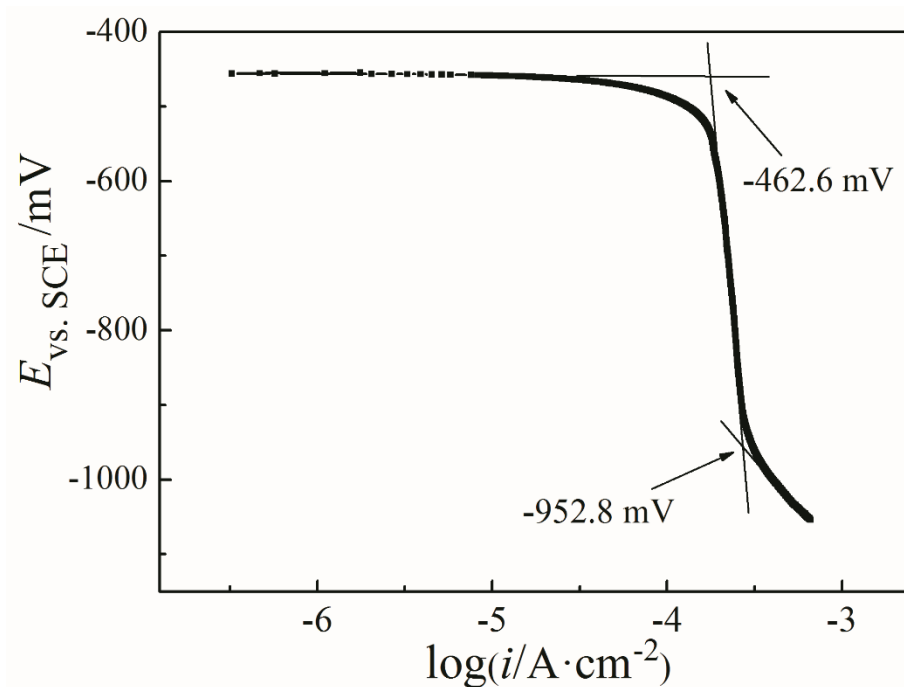


Figure 1. Potentiodynamic polarization curve of X65 steel after initial immersion in seawater containing IOB.

3.2 Weight loss of X65 steel coupons

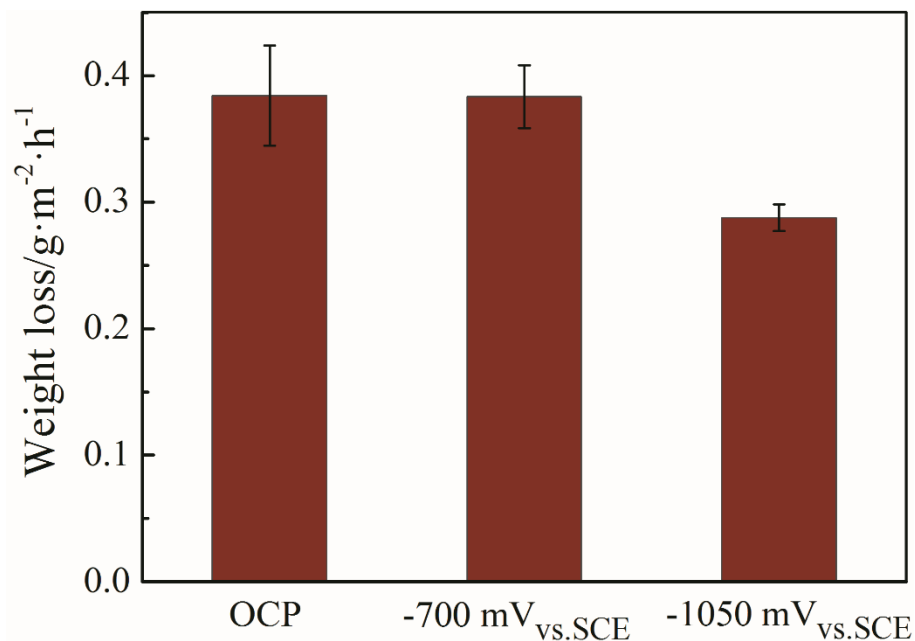


Figure 2. Weight loss of X65 steel immersed in IOB medium for 21d under various cathodic potentials.

The weight loss of X65 steel immersed in seawater containing IOB under various cathodic potentials was presented in Fig. 2. It can be seen that the corrosion rate under $-700 \text{ mV}_{\text{vs. SCE}}$ ($0.3834 \text{ g}\cdot\text{m}^{-2}\cdot\text{h}^{-1}$) was not significantly different from that under OCP (No protection, $0.3841 \text{ g}\cdot\text{m}^{-2}\cdot\text{h}^{-1}$). In

sharp contrast, the X65 steel under $-1050 \text{ mV}_{\text{vs. SCE}}$ ($0.2876 \text{ g}\cdot\text{m}^{-2}\cdot\text{h}^{-1}$) suffered significantly lower corrosion rate than that under OCP. This suggested that $-700 \text{ mV}_{\text{vs. SCE}}$ was not valid to protect the steel from MIC, the potential of $-1050 \text{ mV}_{\text{vs. SCE}}$ should provide effective protection for X65 steel in the presence of IOB.

3.3 Morphology and composition characterization

Surface morphologies of X65 steel in IOB medium under various cathodic potentials were presented in Fig. 3. Under OCP, thick corrosion products along with IOB cells were observed on the coupon surface.

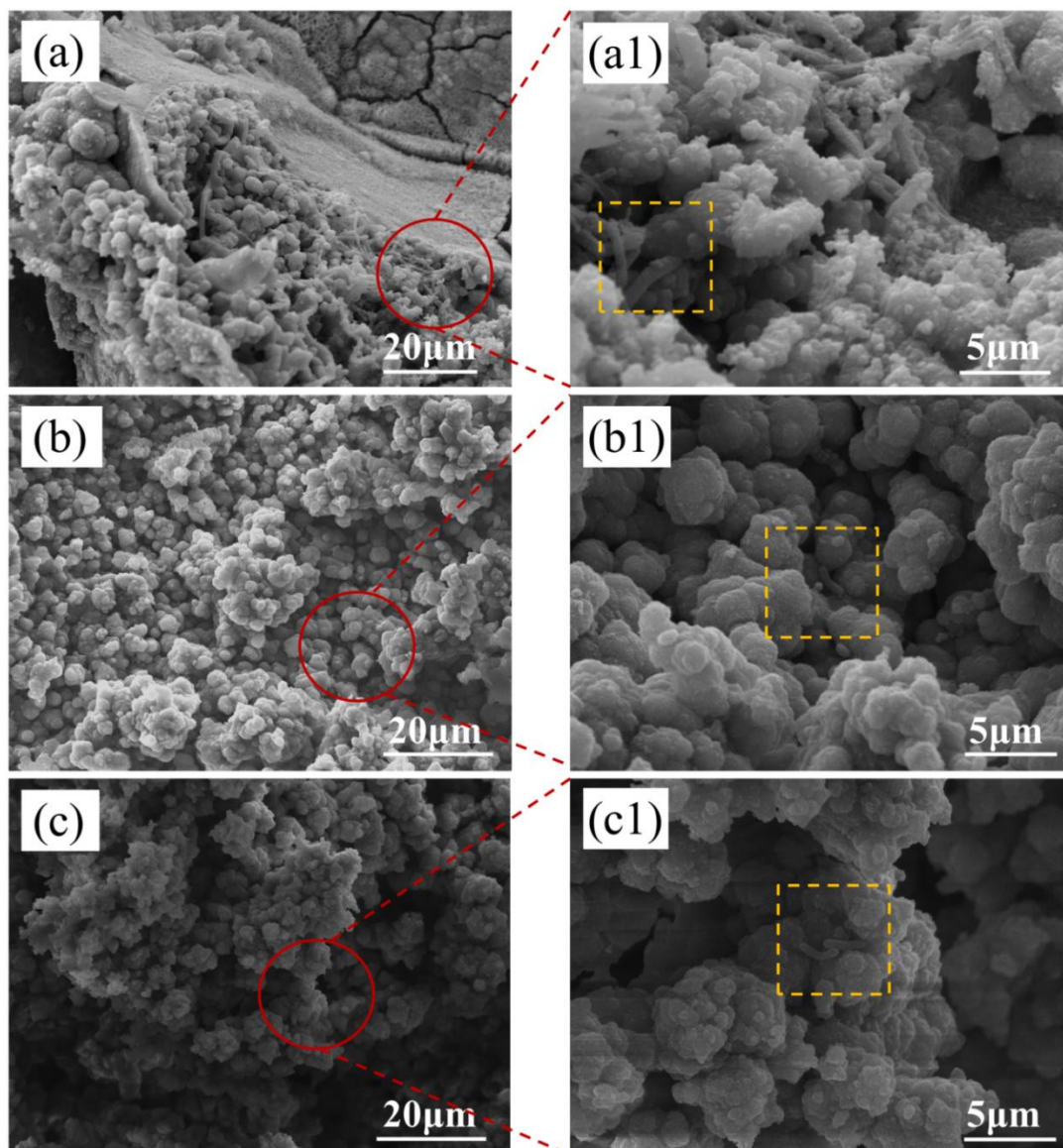


Figure 3. SEM images of X65 steel immersed in IOB medium for 21d under various cathodic potentials: (a, a1) OCP; (b, b1) potentiostatically polarized at $-700 \text{ mV}_{\text{vs. SCE}}$; (c, c1) potentiostatically polarized at $-1050 \text{ mV}_{\text{vs. SCE}}$.

Table 1. EDS analysis results of corrosion products on X65 steel under various cathodic potentials.

Applied potential	Fe	O	C	Ca	Mg	Na	Cl	P	K
OCP	41.05	29.25	14.46	1.73	0.46	1.88	-	10.77	0.41
-700 mV vs. SCE	50.74	30.08	8.22	1.08	0.15	0.72	-	9.00	-
-1050 mV vs. SCE	33.86	33.33	13.88	2.39	0.69	3.30	0.47	11.65	0.64

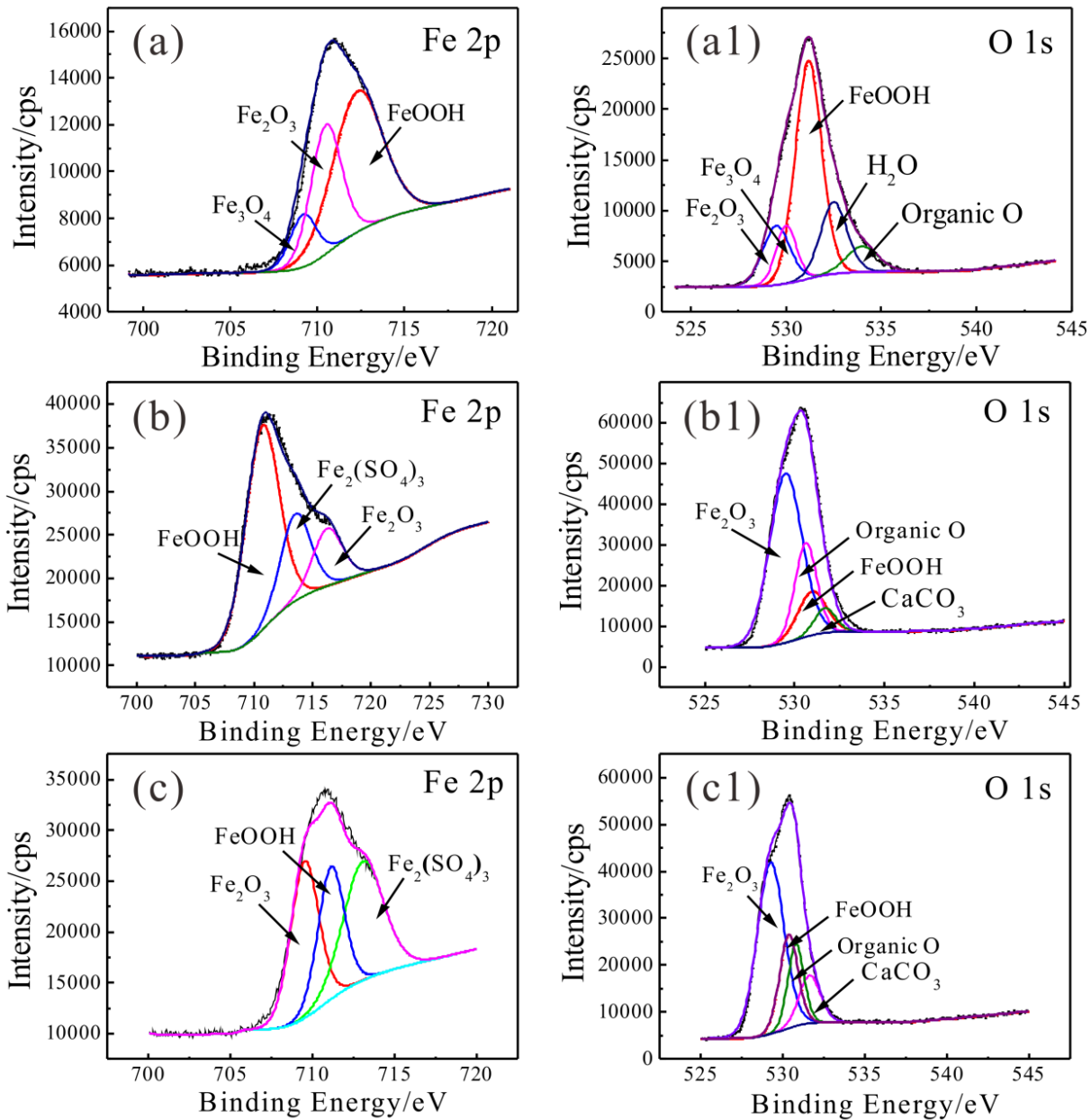


Figure 4. XPS spectra of X65 steel immersed in IOB medium for 21d under various cathodic potentials: (a, a1) OCP; (b, b1) potentiostatically polarized at -700 mV vs. SCE; (c, c1) potentiostatically polarized at -1050 mV vs. SCE.

From the enlarged view in Fig. 3a1, a great number of IOB cells embedded in the biofilm and corrosion products. Under $-1050\text{ mV}_{\text{vs. SCE}}$ (Fig. 3c), few IOB cells were still present in the corrosion products. Moreover, the composition of the corrosion products under $-1050\text{ mV}_{\text{vs. SCE}}$ was notably different from that under the potential of OCP and $-700\text{ mV}_{\text{vs. SCE}}$. The EDS analytical results (Table 1) showed that the corrosion products under $-1050\text{ mV}_{\text{vs. SCE}}$ contained more Ca and Mg elements, indicating the formation of calcareous deposits on the electrode surface. Previous studies have confirmed that when the polarization potential was sufficiently negative, the increase of the interfacial pH on the electrode surface was sufficient for the deposition of calcium and magnesium ions, thereby forming a calcareous deposit layer and providing a protective barrier for the metal [12].

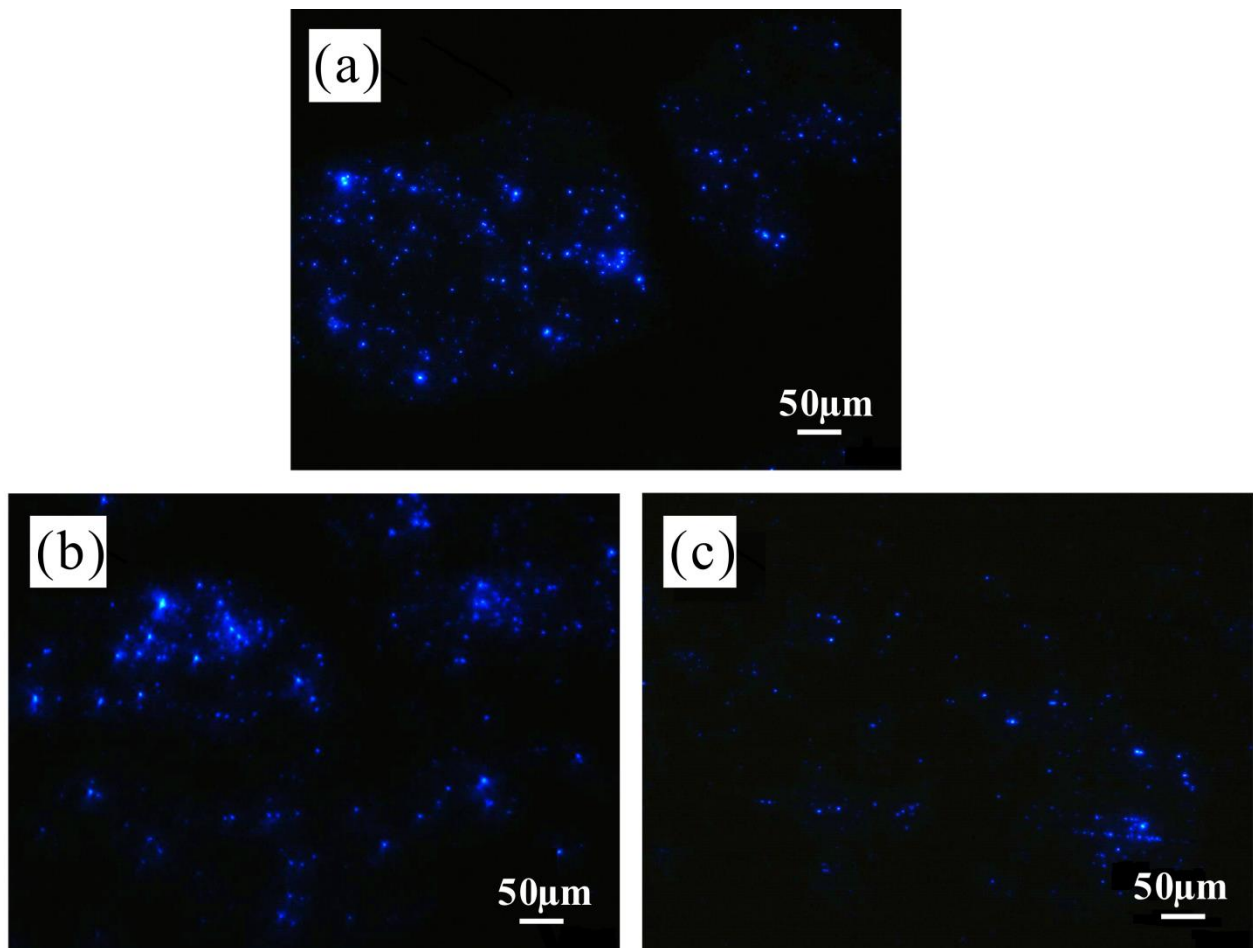


Figure 5. Fluorescence images of X65 steel immersed in IOB medium for 21d under various cathodic potentials: (a) OCP; (b) potentiostatically polarized at $-700\text{ mV}_{\text{vs. SCE}}$; (c) potentiostatically polarized at $-1050\text{ mV}_{\text{vs. SCE}}$.

Fig. 4 showed the XPS analysis for the chemical species of corrosion products under various cathodic polarization potentials. For OCP, the Fe2p spectrum (Fig. 4a) was curve-fitted with three peaks of FeOOH (Binding energy = 712.3 eV), Fe_2O_3 (Binding energy = 710.5 eV) and Fe_3O_4 (Binding energy = 709.2 eV). When cathodic polarization was applied, FeOOH, Fe_2O_3 , and $\text{Fe}_2(\text{SO}_4)_3$ were detected in both coupons but in different proportions, as shown in Fig. 4b and Fig. 4c. The O

spectrum was mainly dominated by FeOOH, Fe₂O₃ and Fe₃O₄. The presence of organic O may be related to EPS produced by IOB. Calcium compound (CaCO₃) only existed under cathodic polarization. And the peak of CaCO₃ (Binding energy = 531.7 eV) under -1050 mV vs. SCE was wider and higher than that under -700 mV vs. SCE. This implied that the OH⁻ associated with the oxygen reduction were increased by the application of cathodic polarization, which in turn resulted in the formation of calcareous deposits on the cathode surface. Furthermore, the more negative cathodic potential (-1050 mV vs. SCE) resulted in more calcareous deposits, which was consistent with the EDS results (Table 1).

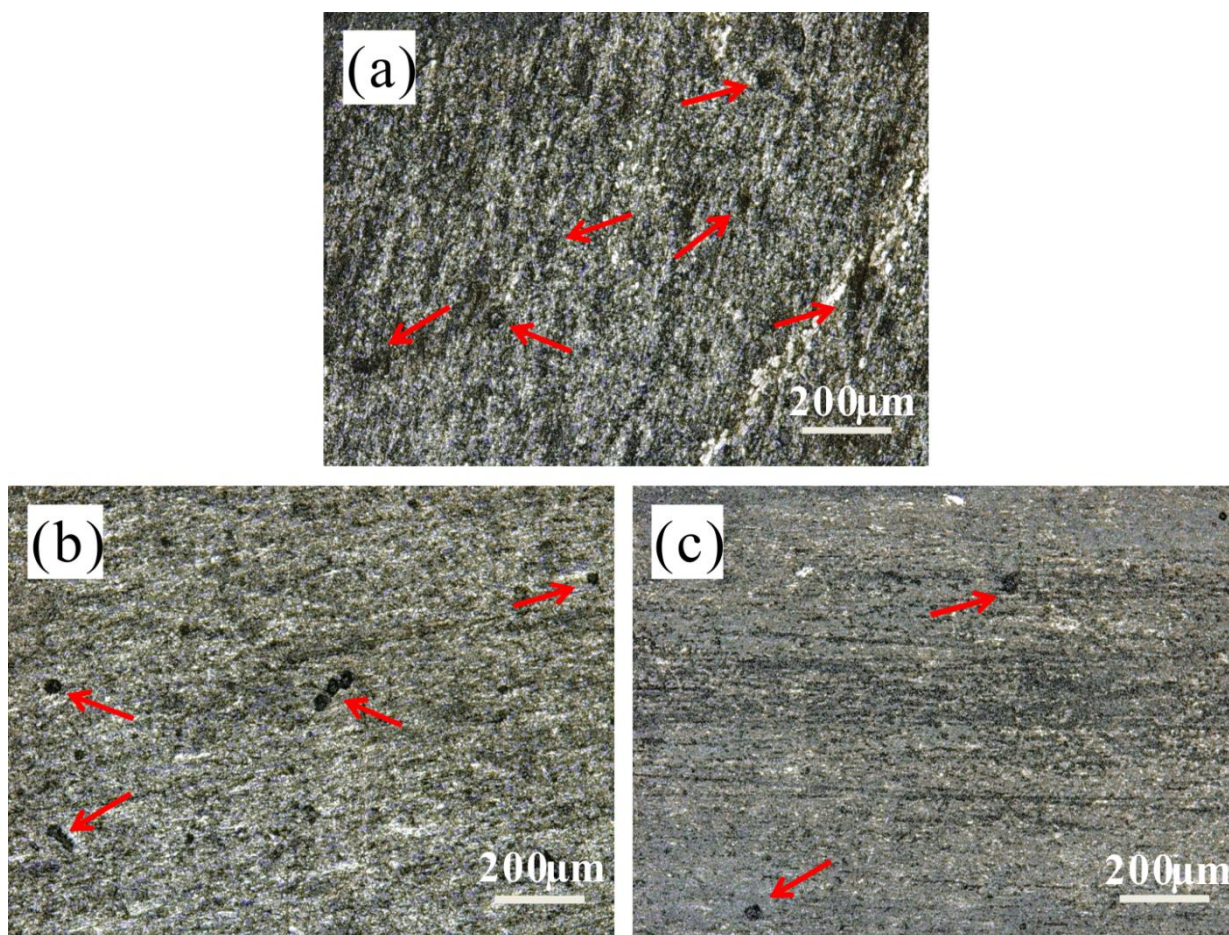


Figure 6. The confocal micrograph of X65 steel immersed in IOB medium for 21d after removing corrosion products under various polarization conditions: (a) OCP; (b) potentiostatically polarized at -700 mV vs. SCE; (c) potentiostatically polarized at -1050 mV vs. SCE.

In order to investigate the role of cathodic polarization on IOB adhesion, Fluorescence detection was performed on bacterial cells attached to the electrode surface under the potential of OCP, -700 mV vs. SCE and -1050 mV vs. SCE, respectively. It can be seen that under OCP (Fig. 5a), a large number of IOB cells attached themselves to the surface of X65 steel for colonization, and formed a biofilm. Compared to unpolarized coupon, the number of bacterial cells did not change significantly under the potential of -700 mV vs. SCE (Fig. 5b). Thus, the applied potential of -700 mV vs. SCE was not

sufficient to affect the settlement and growth of IOB. However, under the negative potential of -1050 mV vs. SCE (Fig. 5c), the attachment of IOB on the electrode surface was significantly reduced. Wilson et al. [13] revealed that gram-negative bacteria had a negative electrostatic surface charge under physiological pH conditions, which can affect the binding of bacterial cells to electrode materials. The polarized surface under -1050 mV vs. SCE was more negatively charged than that under -700 mV vs. SCE. Therefore, IOB cells were repelled by the accumulation of electrons on the steel surface polarized at -1050 mV vs. SCE. There was a great repulsive electrostatic interaction with IOB cells on negatively polarized surface, increasing the resistance of bacterial attachment [7]. The results showed that with the applied potential of -1050 mV vs. SCE, the number of IOB cells was clearly controlled in terms of adhesion.

The surface morphologies of X65 coupon after removing corrosion products were shown in Fig. 6. It was seen that under OCP (Fig. 6a), some IOB-induced pits were formed on the electrode surface. When the protection potential of -700 mV vs. SCE was applied (Fig. 6b), the surface of X65 steel was smooth with some isolated pits. When the potential shifted to -1050 mV vs. SCE (Fig. 6c), the pit size was smaller than that under OCP and -700 mV vs. SCE and the amount of corrosion pits decreased, indicating that the nucleation and growth of pits on the metal surface were inhibited by the polarization potential of -1050 mV vs. SCE.

3.4 Electrochemical studies of X65 steel under various polarization potentials

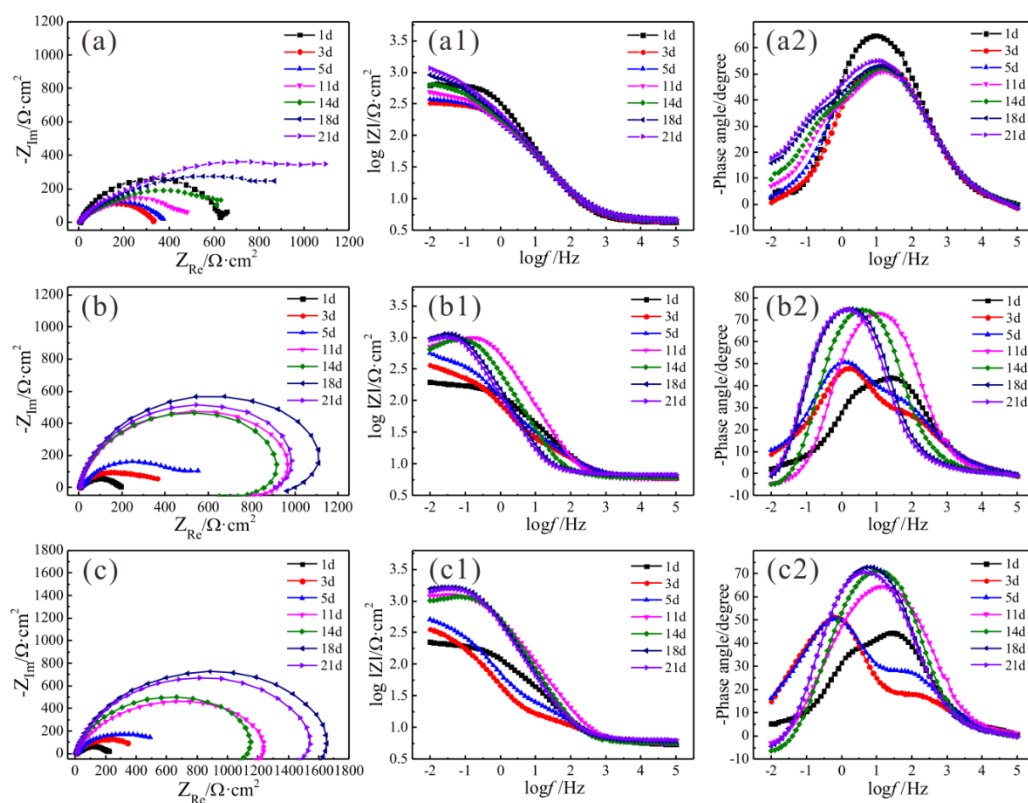


Figure 7. The EIS spectra of X65 steel in IOB medium under various cathodic potentials: (a, a1 and a2) OCP; (b, b1 and b2) potentiostatically polarized at -700 mV vs. SCE; (c, c1 and c2) potentiostatically polarized at -1050 mV vs. SCE.

EIS measurements were performed under various cathodic potentials, as shown in Fig. 7. To show the formation of biofilm and corrosion products on the electrode surface, all experimental data were analyzed with the equivalent circuit containing two-time constants as shown in Fig. 8.

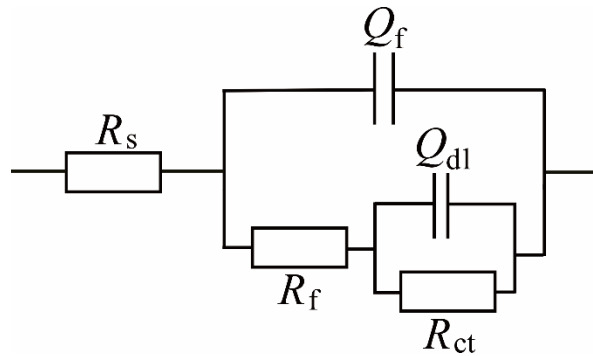


Figure 8. Equivalent circuit used for fitting the EIS results.

Table 2. Electrochemical parameters fitted from the EIS data of X65 steel in IOB medium under various cathodic potentials.

Applied potential	t/d	R_s $\Omega \cdot \text{cm}^2$	C_f $\mu\text{F} \cdot \text{cm}^{-2}$	n_1	R_f $\Omega \cdot \text{cm}^2$	C_{dl} $\mu\text{F} \cdot \text{cm}^{-2}$	n_2	R_{ct} $\Omega \cdot \text{cm}^2$
OCP	1	4.36	677.08	0.77	1610.00	486.68	0.87	633.10
	3	4.41	1070.70	0.70	355.40	953.06	0.78	317.10
	5	4.34	1236.40	0.69	320.80	1349.40	0.73	361.90
	11	4.54	1176.50	0.68	348.10	1604.10	0.62	510.20
	14	4.68	1090.20	0.68	446.30	1562.30	0.56	782.70
	18	4.80	1051.70	0.68	570.60	1538.70	0.52	1246.00
	21	4.78	1053.60	0.69	882.40	1388.90	0.54	1589.00
-700 mV vs. SCE	1	5.98	1252.80	0.68	157.90	1366.20	0.68	188.80
	3	5.67	5516.70	0.50	385.00	3100.30	0.62	355.60
	5	5.82	3591.10	0.55	2961.00	2261.80	0.73	523.80
	11	5.85	2733.50	0.79	3067.00	298.91	0.97	979.80
	14	6.20	775.40	0.78	2995.00	600.36	0.95	969.00
	18	6.11	732.09	0.80	3178.69	1168.80	0.93	1262.00
	21	6.69	1301.30	0.77	3679.00	1458.30	0.93	1142.00
-1050 mV vs. SCE	1	5.49	1294.90	0.68	160.30	1665.00	0.66	217.00
	3	5.42	5538.00	0.39	251.63	6055.40	0.72	397.40
	5	5.13	5920.50	0.48	270.10	3947.40	0.72	551.50
	11	5.70	3496.20	0.81	1305.00	367.96	0.77	1328.00
	14	5.76	320.80	0.79	1251.00	321.89	0.88	1202.00
	18	6.26	428.01	0.85	5822.00	373.35	0.89	1734.00
	21	6.33	504.80	0.80	5766.85	455.07	0.88	1623.00

This equivalent circuit corresponds to a simple corrosion system, where R_s , R_{ct} and R_f represent the resistances of electrolyte solution, surface film consisting of corrosion products and biofilm, and charge transfer, respectively, Q_{dl} and Q_f represent constant phase element (CPE) parameters for double charge layer and surface film, respectively [14]. The impedance CPE is expressed as:

$$Z_{CPE} = Y_0^{-1}(j\omega)^{-n} \quad (2)$$

where Y_0 is the magnitude of the CPE, j is the imaginary number, ω is angular frequency in rad/s and n is the dispersion coefficient related to the deviation from the ideal capacitive behavior. The fitting results of equivalent circuit elements were listed in Table 2.

As observed in Fig. 7a, the diameter of Nyquist plots under OCP decreased from 1 to 3d, and then increased gradually from the third day. In contrast, the diameter of Nyquist plots under -1050 mV vs. SCE increased continually and was larger than those under OCP and -700 mV vs. SCE (Fig. 7c), demonstrating that the interfacial characteristics between the electrode and the biofilm was changed by cathodic polarization. The change in R_{ct} observed from the analysis of the electrode impedances reflected the corrosion sensitivity of X65 steel. Under OCP, as seen in Table 2, the R_{ct} value was decreased before 3d, which was related to the high bacterial activity of IOB. After 5d, the R_{ct} value was increased due to the formation of corrosion products. When the potential of -700 mV vs. SCE was applied, no obvious changes in the R_{ct} were observed compared to that under OCP. However, the R_{ct} under the potentials of -1050 mV vs. SCE was larger than that under OCP after 1d, indicating that the anodic dissolution on the metal surface was suppressed. The rapid increase of R_f under -1050 mV vs. SCE was associated with the formation of calcareous deposits on the electrode surface, which was consistent with the EDS results. The decrease of C_f after 5d under -1050 mV vs. SCE further confirmed the formation of thick calcareous deposits [15].

Fig. 9 showed the potentiodynamic polarization curves of X65 steel under various polarization potentials after 21d and the Tafel analysis results were shown in Table 3, where the E_{corr} and i_{corr} represent the corrosion potential and corrosion current density, respectively, β_a and β_c represent the anodic and cathodic Tafel slopes, respectively. Similar to the weight loss results, the i_{corr} obtained under OCP and -700 mV vs. SCE were quite similar. In contrast, the potential of -1050 mV vs. SCE showed more positive E_{corr} and smaller i_{corr} . For the corrosion process, corrosion rate was closely related to the cathodic and anodic reactions [16]. It was observed that cathodic Tafel slope under the potential of -1050 mV vs. SCE was significantly greater than that under OCP and -700 mV vs. SCE, which corresponded to a slowdown in cathode kinetics. The reason may be that, due to the formation of calcareous deposits under -1050 mV vs. SCE, the cathodic reaction was reduced by inhibiting the diffusion of dissolved oxygen to the electrode surface. The potentiodynamic polarization results were consistent with weight loss data (Fig. 2). It was confirmed again that the potential of -1050 mV vs. SCE provided significant protection for X65 steel.

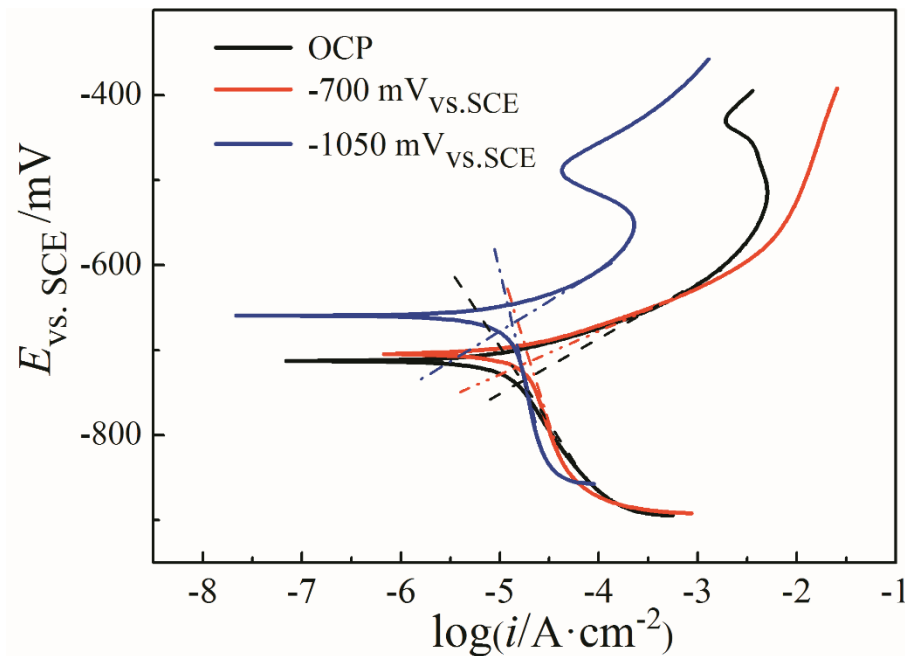


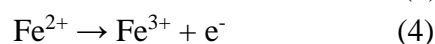
Figure 9. Potentiodynamic polarization curves of X65 steel in IOB medium under various cathodic potentials.

Table 3. Electrochemical parameters fitted from the potentiodynamic polarization curves under various cathodic potentials.

Applied potential	$\beta_a/\text{mV}\cdot\text{dec}^{-1}$	$\beta_c/\text{mV}\cdot\text{dec}^{-1}$	$i_{\text{corr}}/\text{A}\cdot\text{cm}^{-2}$	E_{corr}/V
OCP	61	184	1.52×10^{-5}	-0.74
-700 mV vs. SCE	52	366	1.58×10^{-5}	-0.72
-1050 mV vs. SCE	78	574	1.39×10^{-5}	-0.67

3.5 Inhibition of cathodic polarization on IOB-induced corrosion

The attachment of IOB cells to the surface of X65 steel immersed in seawater solution was strongly affected by the physical and chemical parameters at the electrode interface, which were determined by the intrinsic properties of the interface and the chemical reactions that occurred at the interface. The possible anodic and cathodic reactions occurring at the electrode interface under cathodic polarization in seawater can be described as follows [11]:



Another cathodic reaction that may occur under cathodic polarization in seawater was the formation of H_2O_2 . As described in the literature [17], the cathodic reaction at the electrode interface was related to the degree of electrochemical polarization. Vetter [18] reported that there was a

transition from 2-electron path (6-7) to 4-electron path (5) between the potential range of -400 vs. Ag/AgCl and -800 mV vs. Ag/AgCl:



Therefore, when a potential of -700 mV vs. SCE was applied, the oxygen reduction process at the cathode surface may be accompanied by the generation of H_2O_2 [8]. In the research of electrochemical microbial control, H_2O_2 was considered to be an important factor that caused membrane damage and hindered cell growth [19]. It was worth noting that the presence of oxygen on the cathode surface was essential for the formation of H_2O_2 . But with the prolonged immersion time of X65 steel in seawater, thicker corrosion products accumulated on the coupon surface as shown in Fig. 3b, which hindered the diffusion of oxygen to the electrode surface. Consequently, the production of H_2O_2 was prevented. Fluorescence image (Fig. 5b) showed that the cathodic potential of -700 mV vs. SCE did not affect the attachment of IOB cells on the electrode surface. And weight loss data indicated that the cathodic potential of -700 mV vs. SCE can't provide sufficient protection for X65 steel in the presence of IOB.

Compared to OCP, the number of corrosion pits on the steel surface under -1050 mV vs. SCE decreased sharply as shown in Fig. 6c, indicating that IOB-induced corrosion was inhibited. The decline on the number of corrosion pits was due to the cathodic polarization effect under -1050 mV vs. SCE. With the negative shift of polarization potential from -700 mV vs. SCE to -1050 mV vs. SCE, the strong cathodic polarization potential continuously supplied more electrons to the metal structure, thereby further suppressing the anodic dissolution of metal. The electronic charge applied to the metal surface had an important effect on the attachment of IOB, as schematically shown in Fig. 10. The "electrostatic force" between the polarized surface and the IOB cells depended on the extent of polarization, which can be modified by the cathodic potential, thereby affecting bacterial attachment in seawater. It was supported by our observation that when the X65 steel was sufficiently polarized to -1050 mV vs. SCE, the attachment of IOB cells was significantly suppressed as shown in Fig. 5c.

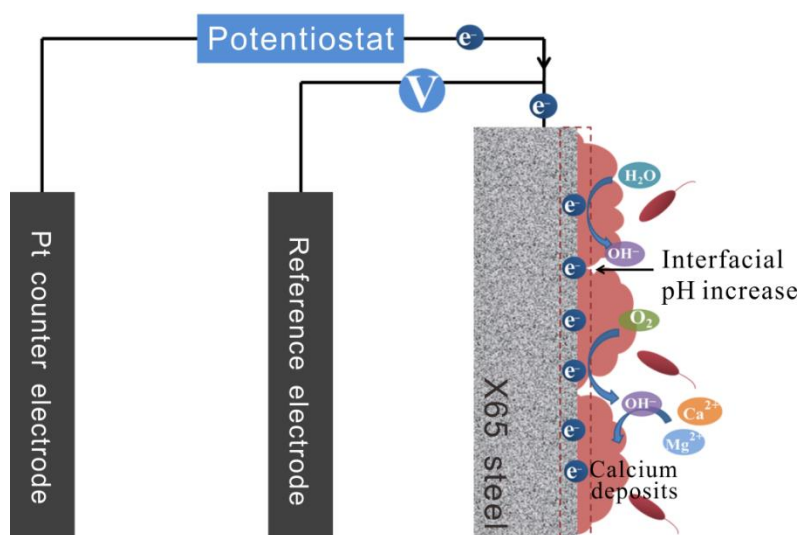
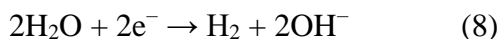
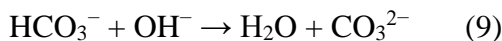


Figure 10. Schematic diagram of the effect of cathodic polarization on attached IOB cells and MIC of X65 steel.

Moreover, the increase of interfacial pH during cathodic oxygen reduction may also be a determining factor for inhibiting bacterial attachment [20]. The surface charge of bacterial cells was related to the pH of the medium, which determined the degree of protonation of ionogenic groups associated with the cell wall [21, 22]. The interfacial pH was increased with the negative shift of cathodic potential, which would make the cell wall negatively charged, thereby enhancing the electrostatic interaction between the bacterial cells and the polarized surface. This work showed that when the potential of $-1050 \text{ mV}_{\text{vs. SCE}}$ was applied, the local pH around the electrode surface was 8.01, which was higher than the optimal pH range for IOB survival. It should be noted that the cathodic potential cannot be too negative, because more negative potential promoted the hydrogen evolution reaction (the reaction below), increasing the risk of hydrogen embrittlement [23].



In addition, the generation of OH^- diminished the solubility of calcium and magnesium ions at the electrode interface, resulting in the precipitation of calcareous deposits, as follows [24]:



The EDS and XPS analytical results (Table 1 and Fig. 4) showed that many calcareous deposits accumulated on the electrode surface under the potential of $-1050 \text{ mV}_{\text{vs. SCE}}$, which acted as a barrier film to offer protection for X65 steel. Therefore, in addition to the role of OH^- , the formation of calcareous deposits also protected X65 steel from IOB-induced corrosion.

4. CONCLUSIONS

In this work, it was demonstrated that the attachment of IOB cells on X65 steel in seawater can be influenced by cathodic polarization. The potential of $-700 \text{ mV}_{\text{vs. SCE}}$ was not sufficient to control the IOB-induced corrosion. However, under the cathodic potential of $-1050 \text{ mV}_{\text{vs. SCE}}$, IOB attachment was inhibited, and the corrosion rate of X65 steel decreased obviously compared with that under OCP. The effect of cathodic polarization on bacterial attachment was attributed to the changes in interfacial properties, such as the charge level of electrode surface, pH and the formation of calcareous deposits, all these comprehensively influenced the attachment of IOB cells, consequently affecting the corrosion process of X65 steel.

ACKNOWLEDGMENTS

This work is supported by National Natural Science Foundation of China (No. 51871204). We are indebted to Jizhou Duan researcher and his team members from Marine Corrosion and Protection Centre, Institute of Oceanology, Chinese Academy of Sciences for their help in microbial culture.

References

1. J. Starosvetsky, D. Starosvetsky, B. Pokroy, T. Hilel, R. Armon, *Corros. Sci.*, 50 (2008) 540.

2. M. Lv, M. Du, *Rev. Environ. Sci. Biotechnol.*, 17 (2018) 431.
3. H. Wang, L.K. Ju, H. Castaneda, G. Cheng, B.M.Z. Newby, *Corros. Sci.*, 89 (2014) 250.
4. M. Moradi, J. Duan, H. Ashassi-Sorkhabi, X. Luan, *Corros. Sci.*, 53 (2011) 4282.
5. Y. Yue, M. Lv, M. Du, *Mater. Corros.*, 70 (2019) 1852.
6. S. Shim, S.H. Hong, Y. Tak, J. Yoon, *Biofouling*, 27 (2011) 217.
7. S.H. Hong, J. Jeong, S. Shim, H. Kang, S. Kwon, K.H. Ahn, J. Yoon, *Biotechnol. Bioeng.*, 100 (2008) 379.
8. R. Babić, M. Metikoš-Huković, *J. Appl. Electrochem.*, 23 (1993) 352.
9. G.A. DeQueiroz, D.F. Day, *J. Appl. Microbiol.*, 103 (2007) 794.
10. O. Istanbulu, J. Babauta, H. Duc Nguyen, H. Beyenal, *Biofouling*, 28 (2012) 769.
11. M. Eashwar, G. Subramanian, S. Palanichamy, G. Rajagopal, S. Madhu, P. Kamaraj, *Biofouling*, 25 (2009) 191.
12. C. Deslouis, D. Festy, O. Gil, V. Maillot, S. Touzain, B. Tribollet, *Electrochim. Acta*, 45 (2000) 1837.
13. W.W. Wilson, M.M. Wade, S.C. Holman, F.R. Champlin, *J. Microbiol. Meth.*, 43 (2001) 153.
14. M. Lv, M. Du, X. Li, Y. Yue, X. Chen, *J. Mater. Res. Technol.*, 8 (2019) 4066.
15. J.H. Kim, Y.S. Kim, J.G. Kim, *Ocean. Eng.*, 115 (2016) 149.
16. D. Örneke, T.K. Wood, C.H. Hsu, F. Mansfeld, *Corros. Sci.*, 44 (2002) 2291.
17. S.T. Sultana, J.T. Babauta, H. Beyenal, *Biofouling*, 31 (2015) 745.
18. K.J. Vetter, *Electrochemical kinetics: theoretical and experimental aspects*, Academic Press (1967).
19. W.K. Liu, M.R. Brown, T.S. Elliott, *J. Antimicrob. Chemother.*, 39 (1997) 687.
20. M. Pérez, C.A. Gervasi, R. Armas, M.E. Stupak, A.R. Di Sarli, *Biofouling*, 8 (2009) 27.
21. R.G.J. Edyvean, A.D. Maines, C.J. Hutchinson, N.J. Silk, L.V. Evans, *Int. Biodeter. Biodegr.*, 29 (1992) 251.
22. B. Little, P. Wagner, D. Duquette, *Corrosion*, 44 (1988) 5.
23. T. Wu, M. Yan, D. Zeng, J. Xu, C. Sun, C. Yu, W. Ke, *J. Mater. Sci. Technol.*, 31 (2015) 413.
24. C. Li, M. Du, R. Gao, *J. Ocean Univ. China*, 16 (2017) 243.